Resonator with Ultrahigh Length Stability as a Probe for Equivalence-Principle-Violating Physics

E. Wiens, A. Yu. Nevsky, and S. Schiller*
Institut für Experimentalphysik, Heinrich-Heine-Universtität Düsseldorf, 40225 Düsseldorf, Germany
(Received 25 September 2016; published 29 December 2016)

In order to investigate the long-term dimensional stability of matter, we have operated an optical resonator fabricated from crystalline silicon at 1.5 K continuously for over one year and repeatedly compared its resonance frequency f_{res} with the frequency of a GPS-monitored hydrogen maser. After allowing for an initial settling time, over a 163-day interval we found a mean fractional drift magnitude $|f_{\mathrm{res}}^{-1} df_{\mathrm{res}}/dt| < 1.4 \times 10^{-20}/\mathrm{s}$. The resonator frequency is determined by the physical length and the speed of light and we measure it with respect to the atomic unit of time. Thus the bound rules out, to first order, a hypothetical differential effect of the Universe's expansion on rulers and atomic clocks. We also constrain a hypothetical violation of the principle of local position invariance for resonator-based clocks and derive bounds for the strength of space-time fluctuations.

DOI: 10.1103/PhysRevLett.117.271102

In this Letter, we address experimentally the question about the intrinsic time stability of the length of a macroscopic solid body. This question is related to the question about time variation of the fundamental constants and effects of the expansion of the Universe on local experiments. It may be hypothesized that, in violation of the Einstein equivalence principle (EP), the expansion affects the length of a block of solid matter and atomic energies to a different degree. The length, defined by a multiple of an interatomic spacing, can be measured by clocking the propagation time of an electromagnetic wave across it. This procedure effectively implements the Einstein light clock or, in modern parlance, an electromagnetic resonator. The hypothetical differential effect would show up as a time drift of the ratio of the frequency f_{res} of an electromagnetic resonator and of an atomic (or molecular) transition (f_{atomic}). A resonator and an atom are dissimilar in the sense that the former's resonance frequency intrinsically involves the propagation of an electromagnetic wave, while the latter does not. Specifically, the time drift would violate the principle of local position invariance (LPI) of the EP. A natural scale of an effect due to cosmological expansion, here the fractional drift rate $D_{\text{res-atomic}} = (f_{\mathrm{atomic}}/f_{\mathrm{res}})d(f_{\mathrm{res}}/f_{\mathrm{atomic}})/dt$, could be the Hubble constant $H_0 \simeq 2.3 \times 10^{-18}/\mathrm{s}$. Extensive work in the past decade has ruled out that an effect of this order exists between different *atomic and molecular* frequency standards [1].

The suitable regime in which to investigate the dimensional stability of matter is at a cryogenic temperature, when the thermal expansion coefficient and the thermal energy content of matter are minimized. Ideally, during the cooling down and then permanence at a cryogenic temperature, a stable energy minimum of the solid is reached. The expected high dimensional stability and the magnitude of H_0 lead to a challenging measurement problem: how to resolve tiny length changes and how to suppress the influence of extrinsic disturbances. The problem can be addressed by casting the solid matter into an electromagnetic resonator of appropriate shape, by supporting it appropriately, and by measuring its resonance frequency using atomic timekeeping and frequency metrology instruments, which indeed permit ultrahigh measurement precision and accuracy.

Cryogenically operated resonators [2] have been developed for microwave and optical frequencies. These represent a viable approach for realizing oscillators having ultrahigh stability both on short and on long time scales (months). Therefore, they have found applications for tests of the EP [2–7] and as local oscillators in connection with microwave and optical atomic clocks [8,9].

Recent cryogenic microwave sapphire resonators exhibit nonzero fractional drifts ($D = f^{-1}df/dt$) of $-1.7 \times 10^{-18}/\mathrm{s}$ [7] and $4 \times 10^{-19}/\mathrm{s}$ [10] and the lowest value reported was $-1.9 \times 10^{-20}/\mathrm{s}$ during a 9-day long interval [11]. For a sapphire cryogenic optical resonator [12], a mean drift smaller than $6.4 \times 10^{-19}/\mathrm{s}$ was measured [13]. Recently, silicon resonators (first studied in Ref. [14]) were investigated at 123 K [9] and at 1.5 K [15,16]. Silicon's advantages are the availability of single crystals of large size at an affordable cost, its easy machinability, a flexibility in the choice of resonator shape, and superpolished mirror substrates allowing high-reflectivity mirrors. Important properties of silicon resonators, such as the thermal expansion coefficient, thermal response, resonator linewidth, and throughput, have already been described in the references given. The 123 K silicon resonator system exhibited an average drift of less than $5 \times 10^{-19}/\mathrm{s}$ over an interval of 70 d [17].

In earlier work on cryogenic resonators, cryostats using liquid coolants were often employed. With the advent of "dry" cryostats, first applied to optical resonator

experiments in Ref. [5], the operation of cryogenic resonators has become possible with reduced maintenance effort and without the disturbances due to the periodic refill of cryogens, opening up new opportunities. Using this technology, the present study was therefore able to investigate a silicon resonator operated at 1.5 K continuously for 420 d. This low temperature is attractive not only for reducing thermal expansion (and consequently reduced requirements for active temperature stabilization) and thermally activated processes but also for reducing the thermal noise of the resonator's components: spacer, mirror substrates, and mirror coatings [15].

We demonstrate here that a crystalline resonator can exhibit outstanding dimensional stability. This performance can be used to test for EP-violating effects. It also has technological potential as an oscillator with a performance improved compared to the well-established masers.

Overview of the apparatus.—Figure 1 (see also [18]) shows the concept of the experiment, which is an extension of our previous work [15]. A silicon resonator is operated in a pulse-tube cooler (PTC) cryostat with a Joule-Thomson (JT) cooling stage, providing a base temperature of 1.5 K.

The silicon resonator is 25 cm long and consists of a cylindrical spacer and two optically contacted silicon mirror substrates [18]. Its linewidth is 2.0 kHz. The resonator is oriented horizontally and supported by wires inside a copper frame [18]. The supports' symmetry is such

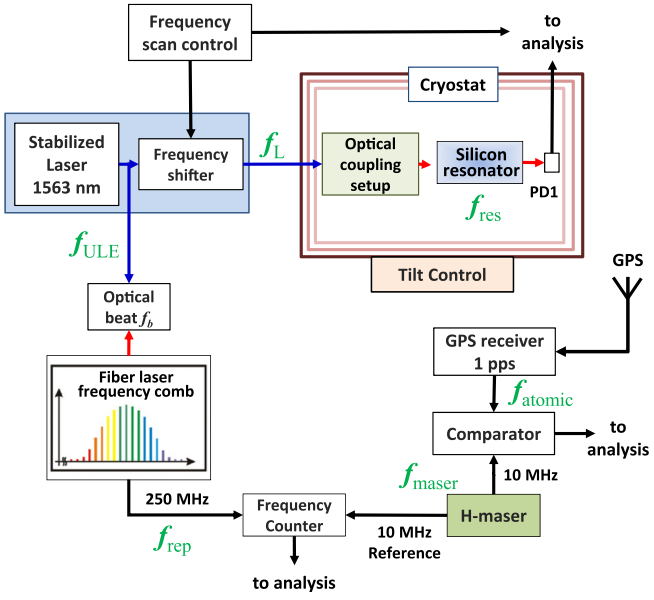

FIG. 1. Principle of the experiment. The optical resonance frequency f_{res} of a silicon resonator is compared with a radio frequency f_{maser} provided by a hydrogen maser. This is done via the intermediary of a laser whose wave of frequency f_L interrogates the resonator and is also measured by an optical frequency comb (pulse repetition rate f_{rep}). The maser frequency is itself compared with a 1-Hz signal (f_{atomic}) obtained from GPS satellites.

that to first order the thermal expansion or length drift of the frame does not affect the resonator length.

In the frequency-scan interrogation technique (Fig. 1), the resonator's TEM_{00} mode frequency f_{res} is read out by a 1.56 μm (192 THz) external-cavity semiconductor laser ("laser 1" in Ref. [18]), which is frequency stabilized to a room-temperature reference resonator (frequency f_{ULE}), having short-time fractional frequency instability 5×10^{-15} and drift 6×10^{-16}/s. During readout, the laser frequency is offset to f_L and is repeatedly scanned in time over a range of a few kilohertz across the silicon resonator resonance (line center frequency f_{res}). We record on the photodetector PD1 the power of the laser wave transmitted through the resonator, fit a line shape model to each scan's data, and extract the frequency offset $f_{\mathrm{res}} - f_{\mathrm{ULE}}$. Simultaneously, the laser frequency corresponding to f_{ULE} is measured by an erbium-fiber-laser-based femtosecond frequency comb, using a hydrogen maser (f_{maser}) as a reference. From these two measurements, we obtain f_{res} in units of f_{maser}. If f_{maser} was constant in time, the long-term variation of f_{res} would mainly be given by the long-term variation of the length l of the silicon crystal resonator spacer and (hypothetically) of the speed of light c, $\Delta f_{\mathrm{res}}/f_{\mathrm{res},0} = \Delta c/c_0 - \Delta l/l_0$, where $f_{\mathrm{res},0}$, l_0, and c_0 are the resonance frequency, the spacer length, and the speed of light at a reference time t_0, respectively.

Systematic effects.—The experiment requires maintaining the operating parameters of the system as stable as possible. Several systematic effects were investigated.

(i) *Temperature.*—The cryostat was operated at its base temperature, and no active temperature stabilization of the resonator was used, since it was unnecessary in the present context. Figure 2 shows the temperature over a period of approximately 420 d with a typical peak-peak variation of 30 mK. The thermal sensitivity of the resonator being $|f_{\mathrm{res}}^{-1} df_{\mathrm{res}}/dT| < 1 \times 10^{-12}$/K at 1.5 K [15,16], this corresponds to a peak-peak fractional frequency deviation $< 4 \times 10^{-15}$, which is not of importance here. On day 327, the operating temperature had to be raised to 1.55 K because of a pressure increase in the JT stage. The calculated shift of 20 Hz was taken into account in the data analysis.

(ii) *Resonator deformation due to gravity.*—The sensitivity to tilt was measured to be $2.5 \times 10^{-16}/\mu$rad and $1.5 \times 10^{-17}/\mu$rad for tilt around the longitudinal and transverse axis, respectively. A tilt control system actuated two of the legs supporting the whole cryostat and reduced the tilt instability to a level below 0.5 μrad for integration times between 100 and 10^4 s.

The time variation of the local gravitational acceleration (tides, etc.) has a negligible effect on the resonator.

(iii) *Laser power.*—The laser power incident onto the resonator during line scan interrogation was 30 μW or less and was not actively stabilized. The power actually coupled into the resonator was 1.5% of the incident power. The power absorbed in the mirror substrate as the laser wave

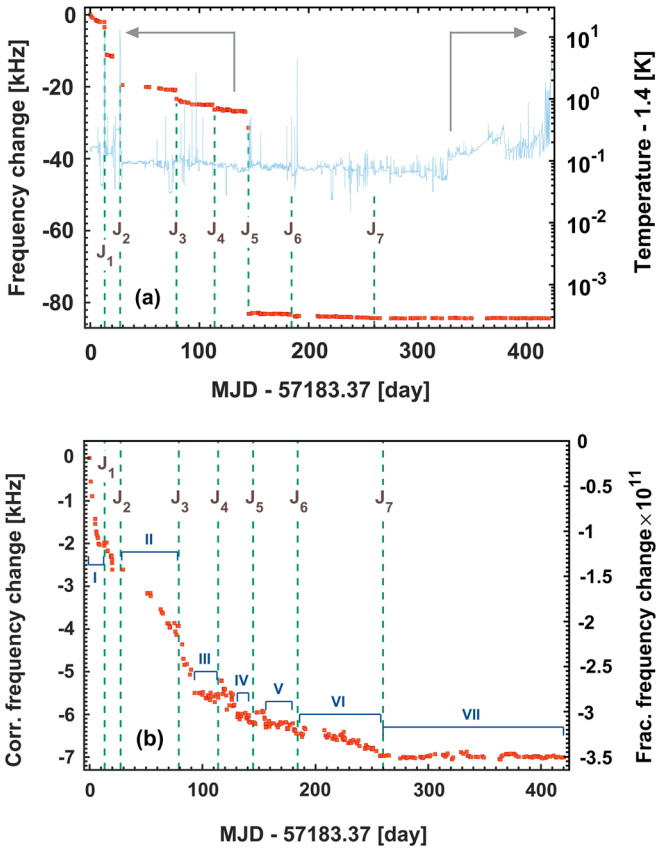

FIG. 2. (a) Variation Δf_{res} of the optical frequency of the silicon resonator (left scale) and its temperature (right scale) over time. During intervals I–VI, the Pound-Drever-Hall locking technique was used. The shown data of interval VII were obtained using the frequency scan technique. Time zero corresponds to the first measurement, performed 4 d after reaching the base temperature (1.5 K). (b) Corrected Si resonator frequency change, obtained by removing frequency jumps that occurred at $J_1, \ldots, J_6$.

traverses it before entering the resonator and the power dissipated inside it could be detected via the concomitant resonator temperature changes. However, the corresponding thermal expansion is negligible. No effect on the resonator frequency could be detected directly.

(iv) *Vibrations.*—They are caused by the periodic (0.7 s) pulsing of the PTC and were characterized at room temperature by motion sensors attached to a plate close to the plate supporting the resonator. All spatial components of the acceleration have complex time evolutions (Fourier frequencies up to a few hundred hertz) and rms values of $(1-8)\times 10^{-3} g$ within a sensor bandwidth of 200 Hz. The accelerations cause resonator deformations that lead to fractional frequency shifts on the order of 10^{-12}, periodic in time. We also performed an interferometric measurement of the periodic axial displacement of a second, identical silicon resonator inside the cryostat. The amplitude is approximately 10 μm.

(v) *Resonator interrogation by the frequency-scan technique.*—This technique (Fig. 1 and Ref. [18]) leads to an Allan deviation of the line center frequency of 2×10^{-14} at 1000 s integration time. During each frequency scan across the resonator mode, the signal recorded by detector PD1 is modulated (25% fractionally) in time in synchronism with the PTC pulsing, probably due to variations in the coupling efficiency caused by the pulsing. The modulation is complex, with pulse-to-pulse variations. These signal disturbances lead to variations of the line center frequencies fitted from individual scans. These variations are of the order 3×10^{-13} (2σ of the data) (gray bars in Fig. 3).

(vi) *Long-term effects of laser light.*—The laser intensity circulating in the resonator might cause photochemical or structural changes in the mirror coatings, with a consequent resonator frequency change. We did not keep any laser frequency resonant for an extended duration, in order to limit the irradiation of the mirrors [18].

(vii) Although it is known that maser frequency drift magnitude can be below 1×10^{-21}/s [20], it is fundamental to determine the influence of our particular maser on the optical frequency measurement. The maser was monitored by comparison with a 1-pulse-per-second signal delivered by GPS, which is derived from the international atomic time scale, defined by the cesium hyperfine transition. During the period days 225–264, the mean fractional drift was 8.2×10^{-21}/s. During the period days 293–415, the mean drift was $D_{\text{maser-GPS}} = 7.5\times 10^{-21}$/s. This level is relevant in comparison with the drift of the resonator's optical frequency with respect to the maser, $D_{\text{res-maser}}$, and thus must be accounted for. The error of $D_{\text{maser-GPS}}$ is negligible for the present discussion.

Measurement of the resonator drift.—Measurements were performed daily, when possible. In practice, each measurement of f_{res} was taken as a time average over several minutes so as to suppress disturbances occurring over short time scales. The long-term behavior of the resonator frequency f_{res} is depicted in Fig. 2(a). Frequency jumps J_1–J_4 were caused by large temperature variations or by unintentional knocks on the cryostat. On day 149 (J_5), we deliberately knocked on the cryostat's outer vacuum chamber and observed a 56 kHz frequency change. The frequency jump after J_6 was probably caused by a power shutdown [18]. To compensate for these jumps, we shifted all frequency values after each jump by an amount equal to the difference between the last measurement before and first measurement after each jump. In Fig. 2(b), we display the resulting time series of the corrected frequency f_{res}, the offsets for $[J_1, \ldots, J_6]$ being $[9.1, 7.8, 2.5, 1.4, 56.1, 0.4] \pm 0.1$ kHz.

We find that, within 2 weeks after each disturbance J_1–J_6, the drift has dropped back to nominally zero. The data intervals III–VI are intervals between frequency jumps during which the resonator remained undisturbed. During these intervals, the drift rates were compatible with zero with upper limits of 4×10^{-19}/s. Interval VII is the period of longest undisturbed duration, 163 d. Starting

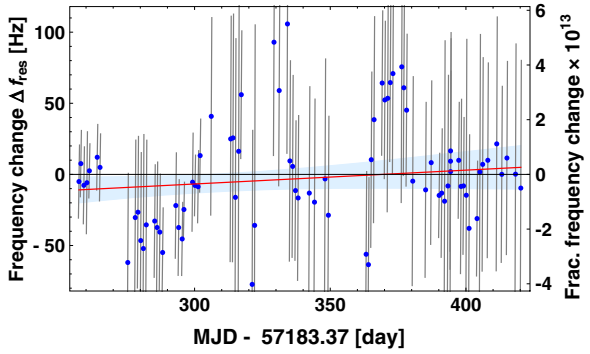

FIG. 3. Resonator optical frequency variation Δf_{res}, corrected for maser drift, during time interval VII, defined in Fig. 2. Each data point (blue) is the average frequency value obtained during a measurement interval i. The bars indicate the range ± twice the standard deviation of each data set i. Red line, time-linear fit, exhibiting a drift rate $D_{\text{res-atomic}} = 5.9 \times 10^{-21}/\mathrm{s}$; blue shaded area, 2σ uncertainty range of the time-linear fit. The zero ordinate value is defined as the mean of the data points.

with this interval, the frequency-scan interrogation technique was used. The f_{res} data thus obtained are shown in Fig. 3. The variations of Δf_{res} are mostly due to the systematic effects (i)–(vi); a possible additional contribution are long-term (time scale of days) maser frequency fluctuations, which we cannot independently identify via GPS, due to the latter's low stability.

Given the long overall measurement duration of 163 d, we can assume that the variations are approximately randomly distributed. A time-linear fit of the optical frequency data f_{res} yields $D_{\text{res-maser}} = (-1.6 \pm 3.8) \times 10^{-21}/\mathrm{s}$ (1σ). We then obtain the drift of the silicon resonator frequency with respect to atomic time as $D_{\text{res-atomic}} = D_{\text{res-maser}} + D_{\text{maser-GPS}} = (5.9 \pm 3.8) \times 10^{-21}/\mathrm{s}$. The systematic effects disturbing the laser frequency scan data and the finite overall measurement time span determine the uncertainty of $D_{\text{res-atomic}}$.

Interpretation.—We interpret the zero drift in three ways: (a) as a test of LPI [2], (b) as a test for effects related to the expansion of the Universe, and (c) as a test of the existence of space-time fluctuations. Local Lorentz invariance is assumed to hold.

(a) One test of LPI is a null clock redshift test that tests for deviations from the clock-type independence of the gravitational time dilation. It consists in measuring the ratio of the frequencies of two dissimilar clocks $C1$ and $C2$, colocated at $\mathbf{r}$, as they are transported through a region of varying gravitational potential $U(\mathbf{r})$. The change of the frequency ratio is written as

$$(f_{C1}/f_{C2})(\mathbf{r}) = (f_{C1}/f_{C2})_0[1 + (\xi_{C1} - \xi_{C2})\Delta U(\mathbf{r})/c^2], \tag{1}$$

where ξ_{C1} and ξ_{C2} are the gravitational coupling constants of the two clock types, $(f_{C1}/f_{C2})_0$ is the frequency ratio measured for the arbitrary reference value U_0, and $\Delta U(\mathbf{r}) = U(\mathbf{r}) - U_0$. If general relativity holds, $\xi = 1$, independent of the type of clock. For two colocated clocks on Earth, $\Delta U(\mathbf{r}) = \Delta U_{\text{solar}}(\mathbf{r})$ is time-varying because of rotational and orbital motion. The Δf_{res} data in Fig. 3 essentially correspond to $\Delta(f_{\mathrm{res}}/f_{\text{atomic}})$, the variation of the ratio of the resonator frequency, and the frequency corresponding to the atomic unit of time (delivered via GPS). A fit of Eq. (1) to the data, neglecting the rotational contribution to ΔU_{solar}, yields $\xi_{\mathrm{res}} - \xi_{\text{atomic}} = (-2.8 \pm 1.6) \times 10^{-4}$ for the clock coupling to the Sun's gravitational potential, which is compatible with zero (the error given is the standard error). The upper bound $|\xi_{\mathrm{res}} - \xi_{\text{atomic}}|_{2\sigma} < 6 \times 10^{-4}$ is nearly equal to the result of Ref. [7] (accounting for the result of Ref. [21]), where a cryogenic microwave sapphire oscillator (CSO) was used. However, our work achieved this result with a measurement duration of 5 months compared to 6 years.

(b) The second interpretation provides a limit for (hypothetical) linear-in-time effects on measuring rods, caused by the expansion of the Universe, if general relativity is violated. Reference [22] discusses that such an effect is absent if general relativity holds. To arrive at such a bound, we first discuss how bounds of LPI violation and time variation of fundamental constants contribute.

We assume that the LPI bound of Refs. [7,21], $|\xi_{\mathrm{CSO}} - \xi_{\text{atomic}}|_{2\sigma} < 5.5 \times 10^{-4}$, holds also for standing-wave optical resonators, like the one used here. This implies that during the interval from day 258 to day 420 the mean resonator drift from a LPI violation is smaller than $|D_{\mathrm{LPI}}|_{2\sigma} = 1.2 \times 10^{-20}/\mathrm{s}$. Note that Ref. [7] derives the LPI bound from the CSO's annual frequency modulation amplitude only. The CSO's frequency drift, $-1.7 \times 10^{-18}/\mathrm{s}$, was removed before data analysis; therefore, the value of D_{LPI} is independent of any expanding-universe effect. Furthermore, we recall that, within conventional physics, $f_{\mathrm{res}}/f_{\text{atomic}}$ (where f_{atomic} is derived from the Cs hyperfine transition) can, in principle, be expressed in terms of the fine-structure constant, m_e/m_p, nuclear parameters, the number of lattice planes in the silicon resonator, and numerical coefficients. The current experimental limits for the drifts of these constants and parameters, derived from comparisons between atomic clocks [1], lead to a bound much smaller than our $|D_{\text{res-atomic}}|_{2\sigma}$ and $|D_{\mathrm{LPI}}|_{2\sigma}$.

Thus, the results of $D_{\text{res-atomic}}$ and D_{LPI} can be combined to set the bound $2.8 \times 10^{-20}/\mathrm{s}$ for the magnitude of linear-in-time drifts of the length of a solid, when measured by effectively clocking the propagation of electromagnetic waves across its length. This is a factor of 82 smaller than the natural scale H_0 and thus rules out any effect that is of first order in H_0.

(c) Space-time fluctuations (or "foam") is a concept that describes the possibility that repeated measurements of a particular time interval or a particular distance do not give a constant result but fluctuate due to fundamental reasons. The measurement of the resonator frequency f_{res}

performed here ultimately corresponds to a measurement of a particular distance (the mirror spacing l_0), in units of the wavelength of an electromagnetic wave resonant with the cesium hyperfine transition. Simple models for the noise power spectral density $S(f)$ (f is the fluctuation frequency) of the fractional length fluctuations $\Delta l/l_0$ have been introduced [23], leading to flicker frequency noise $S_{\text{flicker}}(f) = \alpha/f$ or random-walk frequency noise $S_{\text{rw}}(f) = \beta/f^2$. Experiments are required to place upper limits on α and β.

We compare our time series of f_{res} with simulated time series generated from flicker and random-walk noise and therefrom deduce $S_{\text{flicker}}(f) < 4 \times 10^{-27}/f$ and $S_{\text{rw}}(f) < 9 \times 10^{-33}\ \text{Hz}/f^2$. These limits are weaker than our previous measurements [6,24] but are here established from data at significantly lower Fourier frequencies, $f \simeq 1\ \mu\text{Hz}$.

Summary and outlook.—In this work, we have demonstrated that a silicon crystal exhibits an extremely small length drift at a cryogenic temperature. The mean fractional drift $D_{\text{res-atomic}}$ measured during a time span of 5 months of nearly undisturbed operation was $(5.9 \pm 3.8) \times 10^{-21}/\text{s}$. This is the lowest value measured so far for resonators, to the best of our knowledge. The uncertainty of the value $D_{\text{res-atomic}}$ is due to the systematic effects caused by the cryostat cooler and by the finite measurement time span. Both aspects could be improved in the future. The measurement rules out local consequences of the expansion of the Universe which are of the order of the Hubble constant H_0. In addition, the data provide the best upper limit for violations of local position invariance for an optical resonator and for the existence of space-time fluctuations with frequencies in the μHz range.

To illustrate the smallness of the drift, we note that the 2σ upper limit for $D_{\text{res-atomic}}$, the positive value $1.4 \times 10^{-20}/\text{s}$, is consistent with a shortening of the optical path length in the resonator. If this were caused by the deposition of molecules on the mirrors, the deposition rate would be one molecular layer on each mirror every 3×10^3 years or approximately 30 molecules/s within the laser beam cross section (1 mm diameter).

The cryogenic silicon resonator could potentially be used as a local oscillator with a performance beyond that of hydrogen masers and with autonomous operation. Future progress in cryostat technology may eventually allow suppressing the vibrations to a sufficiently low level so that a silicon resonator exhibits sub-10^{-17} fractional frequency instability, on all time scales, in addition to negligible drift. Until this potential is realized, another suggested implementation consists of a cryogenic silicon resonator combined with an improved version of the ULE-resonator-stabilized laser used here [18]. State-of-the-art ULE resonators are, in principle, capable of providing frequency instability at the 1×10^{-16} level for integration times of up to 1000 s (see, e.g., [25–27]), but this requires eliminating their drift, of typical magnitude $1 \times 10^{-16}/\text{s}$. The drift would be determined by periodic comparison with the silicon resonator and would be compensated by a feedforward scheme. Our work suggests that the proposed solution will be robust and practical, since we showed uninterrupted operation of the resonator for 12 months without serious problems.

We thank I. Ernsting, Q.-F. Chen, U. Rosowski, D. Iwaschko, P. Dutkiewich, and R. Gusek for valuable contributions and M. Schioppo for comments. This work has been funded by European Space Agency Project No. 4000103508/11/D/JR and by Deutsche Forschungsgemeinschaft Project No. Schi 431/21-1.

E. W. and S. S. contributed equally to this work.

*Corresponding author.
step.schiller@hhu.de

[1] J.-P. Uzan, Varying constants, gravitation and cosmology, Living Rev. Relativ. **14**, 2 (2011).
[2] J. P. Turneaure, C. M. Will, B. F. Farrell, E. M. Mattison, and R. F. C. Vessot, Test of principle of equivalence by a null red-shift experiment, Phys. Rev. D **27**, 1705 (1983).
[3] C. Braxmaier, H. Müller, O. Pradl, J. Mlynek, A. Peters, and S. Schiller, Test of Relativity Using a Cryogenic Optical Resonator, Phys. Rev. Lett. **88**, 010401 (2001).
[4] H. Müller, S. Herrmann, C. Braxmaier, S. Schiller, and A. Peters, Modern Michelson-Morley Experiment Using Cryogenic Optical Resonators, Phys. Rev. Lett. **91**, 020401 (2003).
[5] P. Antonini, M. Okhapkin, E. Göklü, and S. Schiller, Test of constancy of speed of light with rotating cryogenic optical resonators, Phys. Rev. A **71**, 050101(R) (2005).
[6] S. Schiller, C. Lämmerzahl, H. Müller, C. Braxmaier, S. Herrmann, and A. Peters, Experimental limits for low-frequency space-time fluctuations from ultrastable optical resonators, Phys. Rev. D **69**, 027504 (2004).
[7] M. E. Tobar, P. Wolf, S. Bize, G. Santarelli, and V. Flambaum, Testing local Lorentz and position invariance and variation of fundamental constants by searching the derivative of the comparison frequency between a cryogenic sapphire oscillator and hydrogen maser, Phys. Rev. D **81**, 022003 (2010).
[8] J. Millo *et al.*, Ultralow noise microwave generation with fiber-based optical frequency comb and application to atomic fountain clock, Appl. Phys. Lett. **94**, 141105 (2009).
[9] T. Kessler, C. Hagemann, C. Grebing, T. Legero, U. Sterr, F. Riehle, M. J. Martin, L. Chen, and J. Ye, A sub-40-mHz-linewidth laser based on a silicon single-crystal optical cavity, Nat. Photonics **6**, 687 (2012).
[10] J. G. Hartnett, N. R. Nand, and C. Lu, Ultra-low-phase-noise cryocooled microwave dielectric-sapphire-resonator oscillators, Appl. Phys. Lett. **100**, 183501 (2012).
[11] J. G. Hartnett, C. R. Locke, E. N. Ivanov, M. E. Tobar, and P. L. Stanwix, Cryogenic sapphire oscillator with exceptionally high long-term frequency, Appl. Phys. Lett. **89**, 203513 (2006).

[12] S. Seel, R. Storz, G. Ruoso, J. Mlynek, and S. Schiller, Cryogenic Optical Resonators: A New Tool for Laser Frequency Stabilization at the 1 Hz Level, Phys. Rev. Lett. **78**, 4741 (1997).

[13] R. Storz, C. Braxmaier, K. Jäck, O. Pradl, and S. Schiller, Ultrahigh long-term dimensional stability of a sapphire cryogenic optical resonator, Opt. Lett. **23**, 1031 (1998).

[14] J.-P. Richard and J. J. Hamilton, Cryogenic monocrystalline silicon Fabry-Perot cavity for the stabilization of laser frequency, Rev. Sci. Instrum. **62**, 2375 (1991).

[15] E. Wiens, Q. Chen, I. Ernsting, H. Luckmann, A. Y. Nevsky, U. Rosowski, and S. Schiller, A silicon single-crystal cryogenic optical resonator, Opt. Lett. **39**, 3242 (2014).

[16] E. Wiens, Q. Chen, I. Ernsting, H. Luckmann, A. Y. Nevsky, U. Rosowski, and S. Schiller, Silicon single-crystal cryogenic optical resonator, Opt. Lett. **40**, 68(E) (2015).

[17] C. Hagemann, C. Grebing, C. Lisdat, S. Falke, T. Legero, U. Sterr, F. Riehle, M. J. Martin, and J. Ye, Ultra-stable laser with average fractional frequency drift rate below 5×10^{-19}/s, Opt. Lett. **39**, 5102 (2014).

[18] See Supplemental Material at, http://link.aps.org/supplemental/10.1103/PhysRevLett.117.271102 which includes Refs. [9, 19], for details of the setup and experimental procedures.

[19] C. Braxmaier, O. Pradl, H. Müller, B. Eiermann, A. Peters, J. Mlynek, and S. Schiller, Fiber-coupled and monolithic cryogenic optical resonators, in *Conference on Precision Electromagnetic Measurements Digest* (IEEE, New York, 2000), pp. 192–193.

[20] D. Matsakis, P. Koppang, and R. M. Garvey, The Long-term stability of the U.S. Naval Observatory's masers, in *Proceedings of the 36th Annual Precise Time and Time Interval Systems and Applications Meeting, Washington, D.C.* (2004), pp. 411–422.

[21] A. Bauch and S. Weyers, New experimental limit on the validity of local position invariance, Phys. Rev. D **65**, 081101 (2002).

[22] S. M. Kopeikin, Optical cavity resonator in an expanding universe, Gen. Relativ. Gravit. **47**, 5 (2015).

[23] Y. J. Ng, Selected topics in Planck-scale physics, Mod. Phys. Lett. A **18**, 1073 (2003).

[24] Q. Chen, E. Magoulakis, and S. Schiller, High-sensitivity crossed-resonator laser apparatus for improved tests of Lorentz invariance and of space-time fluctuations, Phys. Rev. D **93**, 022003 (2016).

[25] Y. Y. Jiang, A. D. Ludlow, N. D. Lemke, R. W. Fox, J. A. Sherman, L.-S. Ma, and C. W. Oates, Making optical atomic clocks more stable with 10^{-16}-level laser stabilization, Nat. Photonics **5**, 158 (2011).

[26] T. L. Nicholson, M. J. Martin, J. R. Williams, B. J. Bloom, M. Bishof, M. D. Swallows, S. L. Campbell, and J. Ye, Comparison of Two Independent Sr Optical Clocks with 1×10^{-17} Stability at 10^3 s, Phys. Rev. Lett. **109**, 230801 (2012).

[27] S. Häfner, S. Falke, C. Grebing, S. Vogt, T. Legero, M. Merimaa, C. Lisdat, and U. Sterr, 8×10^{-17} fractional laser frequency instability with a long room-temperature cavity, Opt. Lett. **40**, 2112 (2015).

Resonator with Ultrahigh Length Stability as a Probe for Equivalence-Principle-Violating Physics: Supplemental Material

E. Wiens, A.Yu. Nevsky, and S. Schiller

Institut für Experimentalphysik, Heinrich-Heine-Universtität Düsseldorf, 40225 Düsseldorf, Germany

Setup details.

Fig. 1 shows the setup of Fig. 1 in the main paper in detail and with an additional laser system. Laser 1 is used for the frequency-scan interrogation of the silicon resonator (the technique shown in Fig. 1 in the main paper), Laser 2 is used for frequency-locking to the silicon resonator using the Pound-Drever-Hall technique (PDH). Similar to the frequency-scan signal, the PDH error signal is also found to be strongly disturbed by the vibrations and also to be influenced by laboratory temperature. In addition, significant residual amplitude modulation is present, which drifts in time. Because the scatter of the f_{res} frequency values obtained by this method was larger than for the frequency-scan method, we base our analysis of the low-drift interval VII on the latter. During intervals I-VI, only PDH data was recorded.

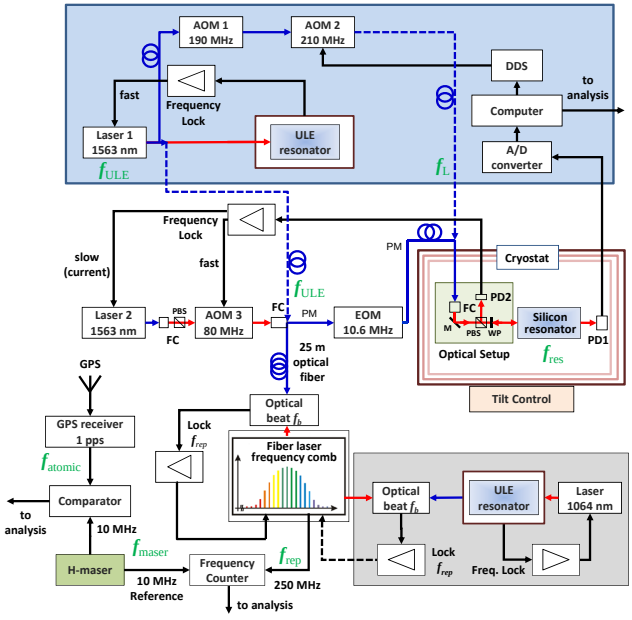

FIG. 1: (Color online). Schematic of the overall setup, containing the silicon resonator, three continuous-wave lasers and an optical frequency comb. To reduce the linewidth of the comb's modes, one of its modes was locked either to a 1.06 μm reference laser (modality A, gray background), to the Si-resonator-stabilized laser (modality B, no colored background), or to a 1.56 μm reference laser (modality C, blue background; dashed blue lines indicate connections when this modality is in use). FC: fiber coupler. AOM: acoustooptic frequency shifter. DDS: Synthesizer. EOM: electrooptic modulator. WP: quarter-wave plate; PBS: polarizing beam splitter. M: set of motorized mirrors. PD1, PD2: photodetectors. Red lines: free-space beams. Blue lines: optical fibers. All r.f. sources are referenced to the H-maser.

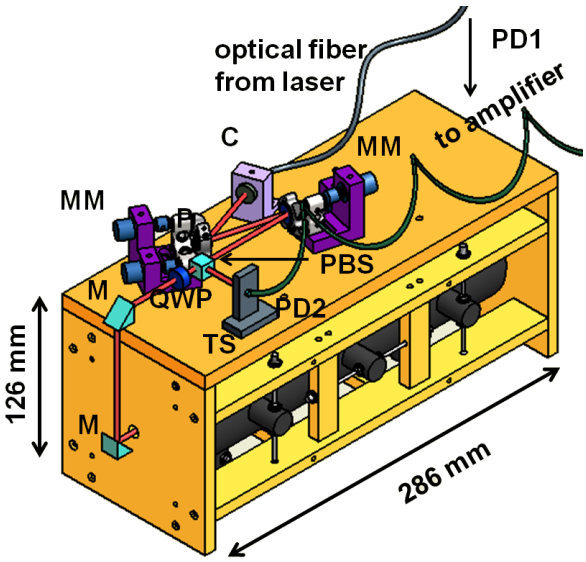

FIG. 2: (Color online). Schematic of the cryogenic resonator (in gray), its holder and the optics breadboard. All shown components are operated at 1.5 K. Laser light is coupled out of a single-mode optical fiber by a collimator C and is guided into the resonator with two motorized mirror mounts MM (for the position adjustment of the beam after cool-down), by a prism P, and a mirror M. Light reflected from the resonator is directed to the cryogenic photodetector PD2 mounted on a two-axis translation stage TS, by the quarter-wave plate QWP and the polarizing beam splitter PBS. The laser light transmitted through the resonator is monitored by photodetector PD1 (not shown). Relative dimensions are to scale.

Fig. 2 shows the cryogenic resonator and its associated optics. We note the difference in the mounting of the resonator in this work and in Ref. [9], where instead it is laying vertically on three columns.

For achieving a coupling of the laser wave into the resonator that is stable in time, it is advantageous to deliver the laser wave to the resonator via a fiber whose outcoupler is rigidly connected with the resonator [19]. In the present setup, wherein the resonator is mounted with wires, the relative alignment of the outcoupler and the resonator changes upon cool-down from room-temperature to cryogenic temperature. In order to be able to compensate for this, we implemented a cryogenic setup, see Fig. 2. It contains two mirrors MM, each actuated by two stepper motors, and a reflection photodetector mounted on a translation stage TS, actuated by two piezo motors.

Optical frequency measurement method and maser.

The measurements of $f_{\rm ULE}$ via the frequency comb are performed by measuring, firstly, the frequency $f_{\rm b}$ of the optical beat between laser and a single comb mode having a frequency near that of the laser and, secondly, the comb's repetition rate $f_{\rm rep} \simeq 250\,$MHz using for the latter a high-resolution counter (see Fig. 1). The carrier-envelope-offset frequency $f_{\rm ceo}$ was stabilized to a synthesizer. The reference frequency signal for the two frequency measurements and the synthesizer is an active hydrogen maser (Vremya-CH VCH-1005).

In order to reduce the linewidth of the comb's modes, with consequent reduction of the noise of the measurement of $f_{\rm rep}$, the comb was optically stabilized. In the course of the experiment, we used three modalities (A, B, C), in which one of the comb's modes was (A) phase-locked to a ULE-reference-cavity-stabilized 1.06 μm laser (days 1 - 132 after cool-down); (B) frequency-locked to the Si-resonator-stabilized laser (days 133 - 415), (C) phase-locked to a ULE-reference-cavity-stabilized 1.56 μm laser (days 257-420). For this purpose, part of the corresponding laser light was sent to the frequency comb, located in a neighboring laboratory, using a 25 m long optical fiber (no phase noise cancellation was implemented). The beat frequency $f_{\rm b}$ was detected with a photodiode and its signal was fed to a servo electronics so as to stabilize it to the value $f_{\rm b} = 50.4$ MHz by acting on the comb's cavity length via an intracavity electrooptic modulator. Under phase-lock conditions, the resulting beat linewidth was $\Delta f_{\rm b} < 1\,$Hz, with a signal-to-noise ratio > 30 dB.

Fig. 3 shows the drift of the maser frequency vs. GPS-delivered 1-pulse-per-second (pps) signals. The mean fractional frequency offset of the maser frequency $f_{\rm maser}$ from 10 MHz was $+1.02\times10^{-11}$, calculated from a linear fit of phase vs. time.

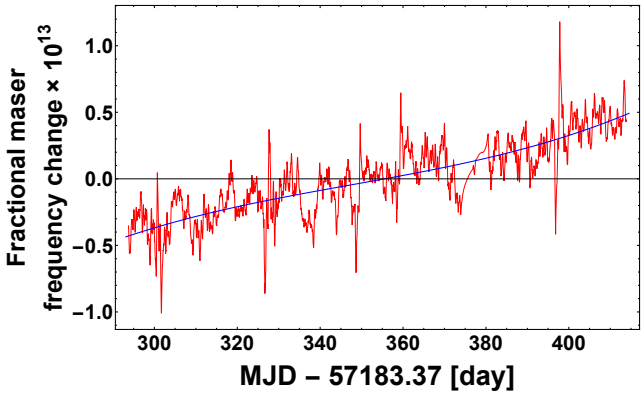

FIG. 3: (Color online) Long-term measurement of the hydrogen maser frequency with respect to atomic time. A GPS receiver provided the phase difference between the maser signal and the GPS signal. Red: maser frequency, computed as 1-day difference quotient of the phase averaged over 6 h. Blue line: maser frequency, computed from a *quartic* fit of the maser-GPS phase difference. The linear-in-time drift rate of the frequency, computed from a *quadratic* fit of the maser-GPS phase difference, is $D_{\rm maser-GPS} = 0.75 \times 10^{-20}$/s. It corresponds to the mean slope of the blue curve. The error is less than 1×10^{-22}/ s. The ordinate value zero corresponds to the mean fractional maser frequency offset, 1.02×10^{-11}.

Operation details.

A pre-alignment of the laser beam exiting the outcoupler was performed while the cryostat was at room temperature. The resonator mode is identified by imaging the light exiting from the backside of the resonator through windows of the cryostat on a room-temperature CCD camera. After cool-down (Fig. 2 in the main paper), a realignment of the beam to the resonator and of the position of the reflection photodetector was necessary. This was done by operating the motors in two steps (for technical reasons), marked J_1 and J_2 in the figures, resulting in a sufficient coupling efficiency into the resonator, at 1.5 K. During both steps J_1 and J_2 (lasting approximately 30 min), the resonator temperature increased to 12 K and 14.5 K respectively, due to the power dissipation in the motor coils, and relaxed back to 1.4 K after several hours. We believe that the resonator frequency change accompanying each realignment was due to relaxation of the resonator after the thermal cycling. No further realignment or changes in the cryogenic setup were performed after day 21.

Most of the temperature peaks in Fig. 2 in the main paper occurred during brief (< 5 min) turn-offs of the cryostat compressor, introduced in order to temporarily eliminate cryostat vibrations and perform measurements of the stabilized laser's linewidth. Furthermore, during the presented measurement campaign three short power black-outs (few min) and one complete power shut-down of the building (30 min) occurred. In order to bridge the latter, we switched to an emergency power generator allowing to keep the compressor operating with only short interruption. However, lasers and electronics were kept off during this time. In anticipation of and during the power shut-down the compressor was off for durations ranging from a few to 10 min, in order to install and test the generator. Several instances of the temperature rise up to 4 K occurred at the end of the measurement period, due to temporary non-function of the Joule-Thomson stage, lasting a few days. We did not observe a residual frequency shift after re-cooling to 1.5 K, within our measurement uncertainty.

In Fig. 2 in the main paper, J_3 and J_4 were caused by unintentional knocks of the cryostat, whereas at J_5 the cryostat was deliberately hit. J_6 was probably caused by a power shut-down and corresponding compensation activities. J_7 marks the reduction of the laser power incident on to the resonator.

Measurements of the frequency $f_{\rm res}$ by the frequency-scan technique and by the PDH technique were performed once per weekday over intervals not longer than 0.5 h. When no measurements were taken, laser 1 (used for the frequency scans) was always blocked. In contrast, until day 327, laser 2 was not blocked but its frequency

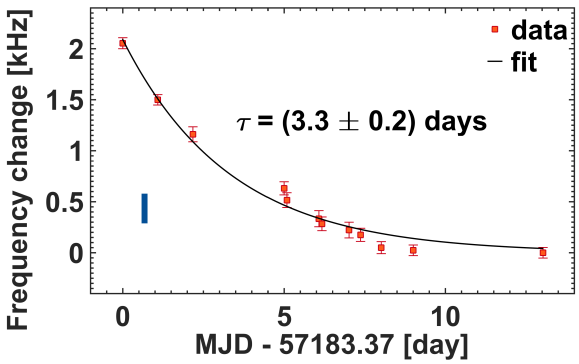

FIG. 4: (Color online) Resonator frequency change $\Delta f_{\rm res}$ during time interval I, starting after first reaching base temperature.

was detuned from resonance. Later, it was also blocked. The power of laser 2 in front of the fiber was approximately 150 μW during intervals I - VI, and was reduced to 60 μW from day 230 on.

Further characterizations.

The interval I of Fig. 2 in the main paper, displayed in more detail in Fig. 4, shows the frequency beginning 4 days after reaching the end of the cool-down, when the resonator temperature had first reached 1.5 K. We find an exponential relaxation of the frequency, with a time constant 3.3±0.2 days, indicating that the resonator and its holder reach equilibrium. In previous cool-down experiments we found values varying between 1.5 and 2.9 days.